Destriping Remote Sensing Image via Low-Rank Approximation and Nonlocal Total Variation

Wenfei Cao, Yi Chang, *Student Member, IEEE*, Guodong Han, and Junbing Li

***Abstract*— Stripe noise removal is a fundamental problem in remote sensing image processing. Many efforts have been made to resolve this problem. Recently, a state-of-the-art method was proposed from image-decomposition perspective. This method argued that the stripe and clear image can be simultaneously estimated by modeling the directional structure of stripes and the local smoothness of remote sensing images. However, the potential of this method cannot be fully delivered when confronting with dense stripes with high intensity. In this letter, we further consider the nonlocal self-similarity of image patches in the spatiospectral volume in terms of nonlocal total variation and propose a method of better robustness to dense stripes. Experimental results on both synthetic and real multispectral data show that the proposed method outperforms other competing methods in the remote sensing image destriping task.**

***Index Terms*— Destriping, low rank, nonlocal total variation (NLTV), spatiospectral volume.**

I. Introduction

REMOTE sensing images [1] normally consist of dozens or even hundreds of spectral bands and have attracted much attention from various application fields, such as mineral detection, urban planning, and precision farming. Unfortunately, the stripes in remote sensing images not only severely degrade the visual quality of images but also limit the related subsequent applications, e.g., image unmixing [2] and classification [3]. Therefore, the destriping issue is a vitally important problem in remote sensing imagery applications.

Many destriping methods with good performance have been developed. These methods can be coarsely categorized into three groups, i.e., statistical-matching-based methods [4], [5], digital-filtering-based methods [6], and variational-model-based methods [7]–[10]. Among these methods, variational-model-based methods are a kind of widely studied approach. Shen and Zhang [7] first proposed the Huber–Markov variational model with spatially local adaptive edge-preserving capacity to remove the stripes. Bouali and Ladjal [8] discovered the directional characteristic of the stripe and proposed a sophisticated unidirectional total variation (UTV) model for single image destriping. However, because of excessive constraint of UTV on the unidirectional derivative, image structural details with the same direction as stripes are inevitably removed. To overcome this drawback, many variants of UTV were proposed (see [11], [12], and references therein). In addition, the destriping methods exploiting the rich spectral information have also been studied. Li *et al.* [13] proposed a multidimensional nonlocal total variation (NLTV) method for suppressing the mixed noise. Zhang *et al.* [9] and He *et al.* [10] presented two low-rank matrix recovery methods in terms of modeling the correlations among spectral bands. For the MODIS-like data, Chang *et al.* [14] developed the anisotropic spatiospectral total variation (ASSTV) method.

Recently, from the image-decomposition perspective, Chang *et al.* [15] proposed a state-of-the-art Low-Rank regularized Image Decomposition (LRID) method for the destriping task. In this letter, recovering stripe and clear image simultaneously is considered as an ill-posed problem, and thus the latent structures of stripe and image are necessarily discovered to regularize the ill-posed problem. More precisely, the directional structure of stripe and the local smoothness of image variations are, respectively, modeled in this letter, leading to a method of outstanding performance. However, when confronting with dense strips with high intensity, the performance of this method might be discounted. In this letter, we further consider the nonlocal self-similarity of patches in the spatiospectral volume and propose a new variational method of better robustness.

II. Problem Formulation and Algorithm

A. Observation Model

Assuming that the stripe is additive, the degradation process due to stripe can be formulated as

$$\mathcal{Y} = \mathcal{X} + \mathcal{S} \tag{1}$$

where $\mathcal{Y} = \{\mathbf{Y}_1, \mathbf{Y}_2, \ldots, \mathbf{Y}_B\}$ is the observed image, with the size of $M \times N \times B$, in which M, N, and B, respectively, indicate the number of the rows, columns, and spectral bands. $\mathcal{X} = \{\mathbf{X}_1, \mathbf{X}_2, \ldots, \mathbf{X}_B\}$ is the original clear image, and $\mathcal{S} = \{\mathbf{S}_1, \mathbf{S}_2, \ldots, \mathbf{S}_B\}$ is the stripe component. The goal of this letter is to simultaneously estimate both the clear image and stripe from the degraded image.

B. Low-Rank Approximation and NLTV Model

Recovering the original clear image and stripe from the degraded image is a highly ill-posed problem. Therefore, some

Manuscript received May 5, 2017; revised August 25, 2017 and October 19, 2017; accepted October 28, 2017. Date of publication March 15, 2018; date of current version May 21, 2018. This work was supported in part by the Natural Science Foundation of China under Grant 61603235 and Grant 61501286 and in part by the Fundamental Research Funds for the Central Universities under Grant GK201603005 and Grant GK201503016. *(Corresponding author: Guodong Han.)*

W. Cao and G. Han are with the School of Mathematics and Information Science, Shaanxi Normal University, Xi'an 710119, China (e-mail: caowenf2015@gmail.com; gdhan.math@gmail.com).

Y. Chang is with the School of Automation, Huazhong University of Science and Technology, Wuhan 430074, China (e-mail: yichang@hust.edu.cn).

J. Li is with the School of Science, Xi'an University of Science and Technology, Xi'an 710054, China (e-mail: fb0618@163.com).

Color versions of one or more of the figures in this letter are available online at http://ieeexplore.ieee.org.

Digital Object Identifier 10.1109/LGRS.2018.2811468

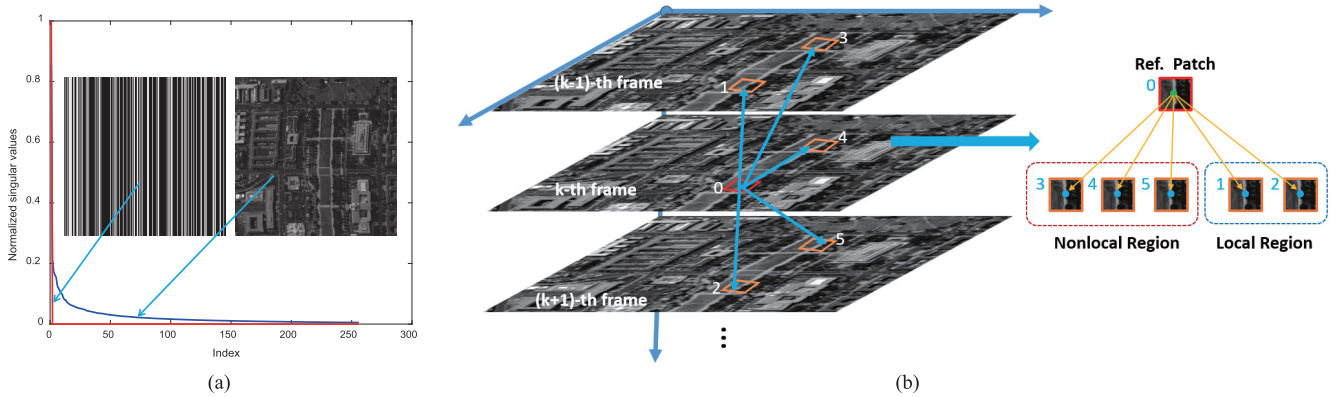

Fig. 1. (a) Curves for the normalized singular values of the stripe and spectral image, respectively. (b) Illustration for the nonlocal self-similarity of image patch and the relationship of the center voxels in local and nonlocal regions.

priori knowledge of the original clear image and stripe is necessarily utilized to regularize the ill-posedness. In the following, we will first discover the priori knowledge of the stripe and original clear image, and then introduce appropriate mathematical modelings of these priors. Finally, by combining the two prior modelings, we propose a new destriping method.

1) Stripe Modeling: The stripes, as demonstrated in [15], are different from the random noises and can be considered as special images with the directional structure. The directional structure implies the low-rank property of band stripes $\mathbf{S}_k$ $(k = 1, 2, \ldots, B)$. As shown in Fig. 1(a), when compared with the dense band images $\mathbf{X}_k (k = 1, 2, \ldots, B)$, the low-rank property of band stripes is significant, which can benefit the estimation of each band stripe. In this letter, matrix nuclear norm, as the tight convex surrogate of rank, is used to characterize the directional structure of each band stripe. Then, the modeling of stripe volume is obtained by a weighted summarization of the nuclear norm of each band stripe

$$\mathrm{LR}(\mathcal{S}) := \frac{1}{B}\sum_{k=1}^{B} \|\mathbf{S}_k\|_* \tag{2}$$

where $\|\mathbf{A}\|_* = \sum_{i=1}^{\min(M,N)} \sigma_i(\mathbf{A})$ indicates the matrix nuclear norm, and $\sigma_i(\mathbf{A})$ stands for the ith singular value of $\mathbf{A}$.

2) Multispectral Image Modeling: The nonlocal self-similarity indicates a phenomenon that a reference patch in an image owns many similar structure patches around it. Fig. 1(b) gives an intuitive illustration. The reference patch marked by a red box possesses five similar patches marked by orange boxes, in which two patches lie in the local region of the reference patch and three patches in the nonlocal region. This powerful priori knowledge has been successfully applied to various image processing tasks [16]. In this letter, this priori knowledge is utilized for the destriping task.

Mathematically, let us denote a reference patch with the center voxel x_r by $\mathbf{P}_r$, denote the center positions of six locally adjacent patches of the reference patch by $\mathcal{D}_1$, and denote the positions of all the voxels in a big $W \times W \times 3$ window around the center voxel x_r by Γ. Then, we can compute the convolution distances between the reference patch and the around patches with their center positions in the set $\Gamma \setminus \mathcal{D}_1$ as the set $\mathcal{S} = \{d_o = \|(\mathbf{P}_o - \mathbf{P}_r) \otimes \mathbf{G}\|_F : o \in \Gamma \setminus \mathcal{D}_1\}$, where $\mathbf{P}_o$ stands for the oth candidate patch with the center voxel x_o, $\mathbf{G}$ is a Gaussian filter of the same size as the reference patch, and $\otimes$ stands for the convolution operation. In practice, the convolution distances can be computed based on a good estimate of the underlying true image. From the distance set $\mathcal{S}$, we can select $m - 6$ smallest distances, which correspond to $m - 6$ similar structure patches in the nonlocal region of the reference patch. After obtaining the m similar structure patches, we can define 3-D nonlocal total variation of the center voxel x_r. For this center voxel, as shown in Fig. 1(b), its nonlocal total variation is formulated as

$$\mathrm{NLTV}(x_r) := \sqrt{\sum_{o\in\mathcal{D}_1} w_o \cdot (x_o - x_r)^2 + \sum_{o\in\mathcal{D}_2} w_o \cdot (x_o - x_r)^2}$$

where $\mathcal{D}_2$ stands for the nonlocal region around the reference patch $\mathbf{P}_r$, the cardinality of $\mathcal{D}_1 \cup \mathcal{D}_2$ is the number m of similar patches, and $w_o (o = 1, 2, \ldots, m)$ is an adaptive weight. Here, w_o is obtained by first computing similar-patch distances in terms of $\exp(-(d_o^2/h^2))$ and then normalizing it, where h is a scale parameter. Then, the 3-D NLTV of the image volume $\mathcal{X}$ can be defined as

$$\mathrm{NLTV}(\mathcal{X}) := \sum_r \mathrm{NLTV}(x_r). \tag{3}$$

Compared with the common 3-D total variation, which only describes local spatiospectral correlation, NLTV considers the integration of local spatiospectral correlation and nonlocal correlation and can give more accurate image restoration.

3) Proposed Model: Combining stripe modeling (2), image modeling (3), and observation model (1), we propose a new variational model for the destriping task as

$$\min_{\mathcal{S}\ \mathcal{X}} \frac{1}{2}\|\mathcal{Y} - \mathcal{S} - \mathcal{X}\|_F^2 + \lambda_1 \mathrm{LR}(\mathcal{S}) + \lambda_2 \mathrm{NLTV}(\mathcal{X}) \tag{4}$$

where λ_1 and λ_2 are the tradeoff parameters. The first term in this model is the fidelity term, and the second and third terms are regularization terms. Here, it is necessary to make a comparison between the proposed model and the LRID model in [15]. The anisotropic total variation in the LRID model is used to describe local intensity variation of the spectral images, while the NLTV in the proposed model describes the

spatiospectral intensity variation in both local and nonlocal regions of the reference patch, and hence can lead to better robustness to the noises, which will be demonstrated in the subsequent experiments.

C. Optimization Algorithm

The optimization model in (4) can be solved by alternatively optimizing $\mathcal{S}$-subproblem and $\mathcal{X}$-subproblem [17].

1) $\mathcal{S}$-subproblem is

$$\min_{\mathcal{S}} \frac{1}{2}\|\mathcal{S}-(\mathcal{Y}-\mathcal{X}^n)\|_F^2+\frac{\lambda_1}{B}\sum_{k=1}^{B}\|\mathbf{S}_k\|_*.$$

This subproblem can be solved by performing B singular value shrinkages

$$\mathbf{S}_k^{n+1} := \text{Shrink}_{\text{trace}}\left(\mathbf{Y}_k-\mathbf{X}_k^n,\frac{\lambda_1}{B}\right)\quad k=1,2,\ldots,B.$$

Here, $\text{Shrink}_{\text{trace}}(\mathbf{A},\lambda) = \mathbf{U}\text{diag}\big(\mathcal{T}_\lambda(\text{diag}(\Sigma))\big)\mathbf{V}^T$, where $\mathbf{U}\Sigma\mathbf{V}^T$ is the singular value decomposition of matrix $\mathbf{A}$ and $\mathcal{T}_\lambda(\cdot)$ is the well-known soft thresholding shrinkage operator.

2) $\mathcal{X}$-subproblem is

$$\min_{\mathcal{X}} \frac{1}{2}\|\mathcal{X}-(\mathcal{Y}-\mathcal{S}^{n+1})\|_F^2+\lambda_2\text{NLTV}(\mathcal{X}).$$

This NLTV regularized denoising problem, according to the work [18], can be solved by an iterative procedure. This iterative procedure can be formally denoted by

$$\mathcal{X}^{n+1} := \text{Shrink}_{\text{nltv}}(\mathcal{Y}-\mathcal{S}^{n+1},\lambda_2).$$

It is worth noting that $\mathcal{X}$ in the above alternative iterations is initialized by the method ASSTV [14], and the positions of the nonlocal similar patches are sought out through the estimated $\mathcal{X}$ and then fixed throughout the iterative procedure.

III. Experiments

In this section, the simulated and real experiments are conducted to demonstrate the effectiveness of the proposed method. All the testing images are normalized into the range [0, 1]. We compared the proposed method, termed as LrNLTV, with the two state-of-the-art destriping methods: ASSTV and LRID [15]. For the simulated experiments, the mean pink signal-to-noise ratio (MPSNR) and mean structure similarity (MSSIM) [19] of spectral band images are selected as the assessment indexes, where a high MPSNR value implies a good recovery performance over the image intensity and a high MSSIM value indicates a good recovery performance over the image structure features. In our method, the number of similar patches m is empirically set as 16 and each patch is of the size 7×7. The window size W is empirically set as 25. The scale parameter h is empirically set as 20. The tradeoff parameters λ_1 and λ_2 are manually adjusted to some value such that our method can achieve best MPSNR values for the testing images. When λ_1 empirically takes a value in the range [0.2, 0.3] and λ_2 a value in the range [0.0075, 0.01], our method LrNLTV will have a good recovery performance.

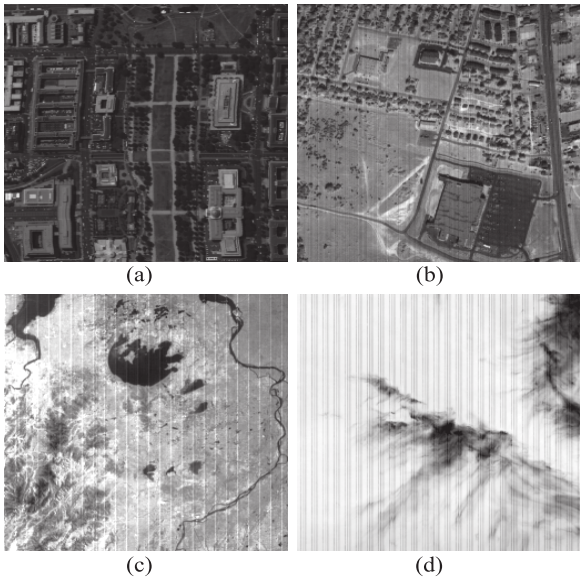

Fig. 2. Testing remote sensing spectral images. Note that only one band image is shown here. (a) For simulated experiments. (b)–(d) For real experiments.

TABLE I
MPSNR (dB) and MSSIM Values of Different Destriping Methods for Periodic Stripes Under Different Noise Levels

Methods	intensity = 50				intensity = 100			
	rt=0.2	rt=0.4	rt=0.6	rt=0.8	rt=0.2	rt=0.4	rt=0.6	rt=0.8
Degrade	21.24 dB 0.5076	18.23 dB 0.3440	16.47 dB 0.2400	15.22 dB 0.1897	15.23 dB 0.2776	12.21 dB 0.1193	10.45 dB 0.0718	9.20 dB 0.0478
LRID	39.77 dB 0.9877	38.94 dB 0.9862	37.97 dB 0.9829	37.71 dB 0.9820	38.37 dB 0.9838	37.35 dB 0.9797	37.71 dB 0.9803	37.52 dB 0.9801
ASSTV	39.54 dB 0.9895	39.04 dB 0.9874	37.72 dB 0.9838	37.27 dB 0.9801	37.46 dB 0.9819	37.28 dB 0.9815	36.76 dB 0.9792	36.05 dB 0.9758
LrNLTV	**40.24 dB** **0.9888**	**39.92 dB** **0.9880**	**39.50 dB** **0.9874**	**39.02 dB** **0.9854**	**39.21 dB** **0.9861**	**39.18 dB** **0.9863**	**38.68 dB** **0.9851**	**38.40 dB** **0.9843**

A. Simulated Experiment Results

The hyperspectral image Washington DC Mall[1] is used as the testing image [see a band image of this image volume in Fig. 2(a)]. The striped images are generated by adding the synthetic stripe via the observed model (1) into the spectral images between band 21 and band 30. The structure of stripes is either periodic or nonperiodic due to the difference of imaging mechanism. We show the quantitative assessment results for periodic and nonperiodic stripes with different noise levels in Tables I and II, respectively. In these two tables, rt denotes the ratio of the stripe area within each band image and $intensity$ means the mean absolute value of the stripe lines.

From these two tables, the following two observations can be obtained. First, when the periodic stripe is added, LRID method produces a bit better recovery results on average than those of the ASSTV method. However, when the nonperiodic stripe is introduced, the ASSTV method works slightly better than the LRID method. Second, our method LrNLTV has a consistently better performance than the two competing methods, which suggests that our method is very robust to

[1] https://engineering.purdue.edu/ biehl/MultiSpec/hyperspectral.html.

TABLE II

MPSNR (dB) AND MSSIM VALUES OF DIFFERENT DESTRIPING METHODS FOR NONPERIODIC STRIPES UNDER DIFFERENT NOISE LEVELS

Methods	intensity = 50				intensity = 100			
	rt=0.2	rt=0.4	rt=0.6	rt=0.8	rt=0.2	rt=0.4	rt=0.6	rt=0.8
Degrade	21.16 dB 0.5628	18.15 dB 0.3630	16.36 dB 0.2523	15.12 dB 0.1905	15.14 dB 0.3415	12.13 dB 0.1452	10.34 dB 0.0724	9.10 dB 0.0405
LRID	36.70 dB 0.9829	34.95 dB 0.9758	34.25 dB 0.9733	33.80 dB 0.9714	33.33 dB 0.9692	31.11 dB 0.9499	30.96 dB 0.9469	30.62 dB 0.9432
ASSTV	37.28 dB 0.9843	36.13 dB 0.9819	35.84 dB 0.9787	34.30 dB 0.9738	34.15 dB 0.9733	33.08 dB 0.9679	31.38 dB 0.9557	30.71 dB 0.9504
LrNLTV	**38.26 dB** **0.9857**	**37.50 dB** **0.9850**	**37.37 dB** **0.9832**	**35.40 dB** **0.9783**	**35.49 dB** **0.9793**	**34.57 dB** **0.9775**	**32.55 dB** **0.9655**	**31.89 dB** **0.9658**

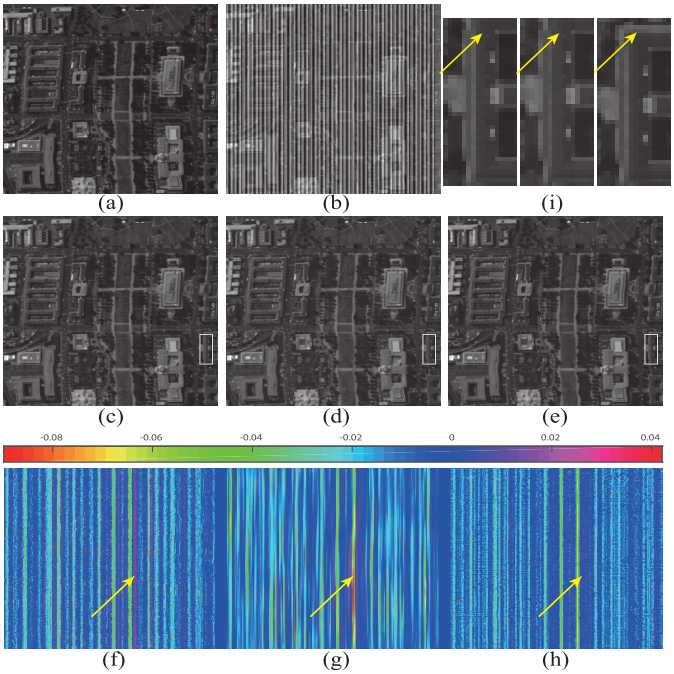

Fig. 3. Destriping results for the periodical stripe case ($r = 0.6$ and intensity $= 100$) in simulated experiments. (a) Original hyperspectral image band 25. (b) Degraded image with periodic stripes. Destriping results by (c) LRID, (d) ASSTV, and (e) LrNLTV. The differences of the recovery image with the original image for (f) LRID, (g) ASSTV, and (h) LrNLTV. (i) Detailed regions cropped from (c)–(e).

the dense stripe with high intensity. This observation is not surprising. This is because when compared with these two methods, our method considers the self-similarity property in the nonlocal region besides the local smoothness of spectral images, and the modeling of this additional information can enhance the robustness of our method.

We also exhibit the subjective recovery results in Figs. 3 and 4. It can be seen, from Fig. 3(f)–(h), that the difference of the recovery image with the original one for our method LrNLTV is visually not very large and more close to zero than those for the methods LRID and ASSTV, especially as the yellow arrows indicate. This finding reveals that the recovery result of our method is the best of all compared methods. Moreover, from the detailed regions of Fig. 3(i), it can be observed that the recovery results of the methods LRID and ASSTV are blurred, whereas our method gives a relatively sharp result. In addition, the estimation accuracy of stripes is also a good index for evaluating the

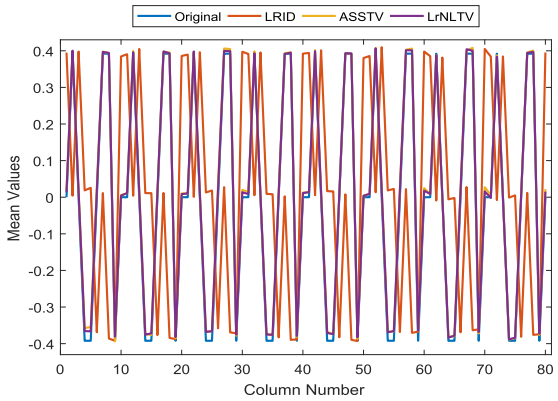

Fig. 4. Mean value comparison between the stripes estimated by LRID, ASSTV, LrNLTV, and the original one ($r = 0.6$ and intensity $= 100$).

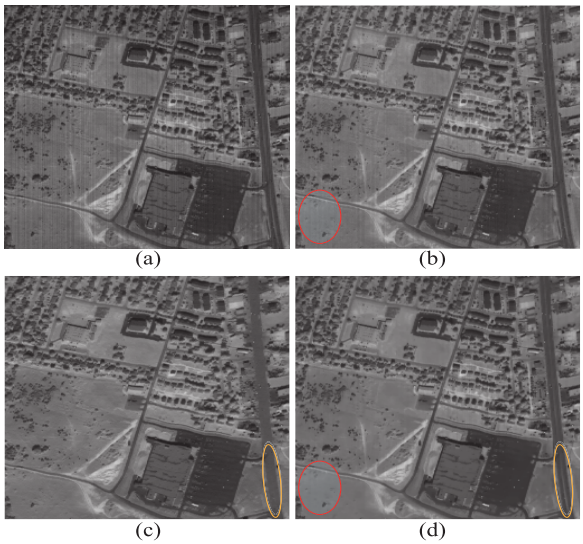

Fig. 5. Destriping results for the HYDICE image with the nonperiodical stripe. (a) Original image band 103. Destriping results by (b) LRID, (c) ASSTV, and (d) LrNLTV.

recovery performance of destriping methods. Fig. 4 gives the mean values of the estimated and original stripes in the first 80 columns. From this figure, we can observe that the estimate stripe by our method LrNLTV is more matched to the original stripe than the other two methods, which implies that the proposed method is of better recovery capacity.

B. Real Experiment Results

We further conduct real experiments to justify the effectiveness of the proposed method. The testing image volumes of size $256 \times 256 \times 6$ were extracted from one HYDICE image[2] with the nonperiodic stripe and two MODIS images[3] with the periodic stripe, one band image of which is, respectively, shown in Fig. 2(b)–(d).

Fig. 5 shows the destriping results for the HYDICE image with the nonperiodic stripe, and Figs. 6 and 7 exhibit the destriping results for the MODIS image with the moderate and heavy periodic stripe, respectively. From Fig. 5, it can be seen that the recovery image of the LRID method, as the red

[2]http://www.tec.army.mil/hypercube.

[3]https://ladsweb.modaps.eosdis.nasa.gov/.

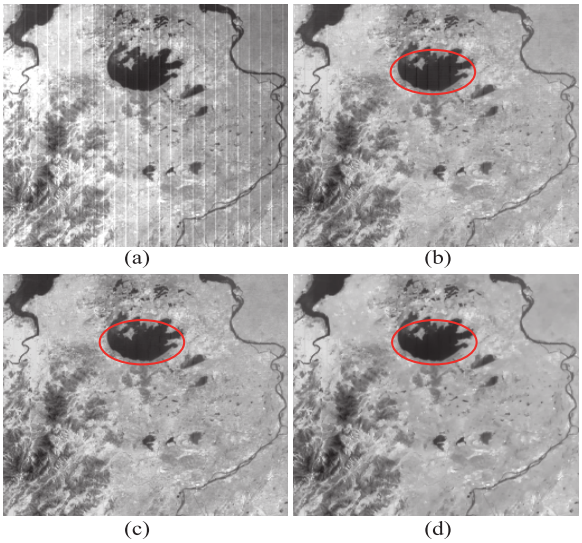

Fig. 6. Destriping results for the MODIS image with the moderate periodical stripe. (a) Original image band 30. Destriping results by (b) LRID, (c) ASSTV, and (d) LrNLTV. It would be better to see this figure by zooming on a computer screen.

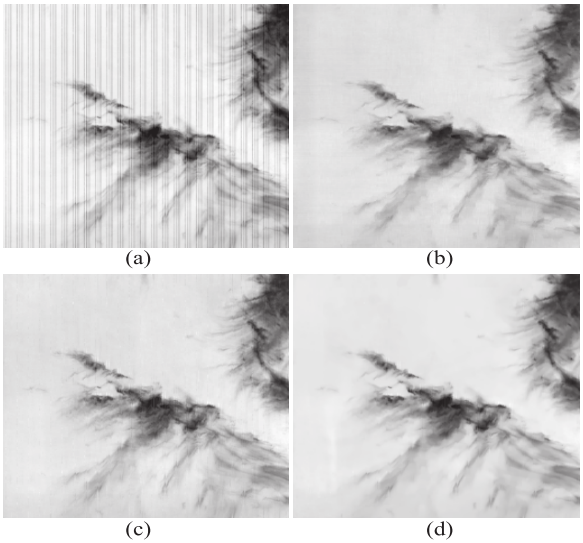

Fig. 7. Destriping results for the MODIS image with the heavy periodical stripe. (a) Original image band 28. Destriping results by (b) LRID, (c) ASSTV, and (d) LrNLTV.

elliptical box indicates, contains a little weak stripes, and some recovery regions of the ASSTV method are oversmoothed, e.g., the white traffic marking in the middle of the highway, whereas the LrNLTV method overall gives a visually clear and sharp recovery image. The reason might be that the LRID and ASSTV methods only model the local smoothness in terms of spatiospectral total variation, whereas our method LrNLTV considers the additional self-similarity information in the nonlocal region of images, which can boost the robustness and recovery performance. Similar observations can be obtained from Figs. 6 and 7.

IV. Conclusion

In this letter, we proposed an NLTV and low-rank regularized variational model for destriping remote sensing images. In this model, each band stripe matrix is considered as a special image with low-lank constraint. The NLTV is then employed to describe the spatiospectral intensity variation of spectral images in the local and nonlocal regions of the reference patch. Because of the introduction of the nonlocal region information of images, the proposed method has a better robustness over other competing methods. Experimental results on the simulated and real data reveal that the proposed method outperforms two state-of-the-art destriping methods in terms of the objective and perceptual qualities. In the future work, our effort will be devoted to a fast implementation of the proposed method in the graphic processing unit architecture.

References

[1] J. A. Richards and X. Jia, *Remote Sensing Digital Image Analysis: An Introduction*, 4th ed. Berlin, Germany: Springer-Verlag, 2006.
[2] M.-D. Iordache, J. Bioucas-Dias, and A. Plaza, "Sparse unmixing of hyperspectral data," *IEEE Trans. Geosci. Remote Sens.*, vol. 49, no. 6, pp. 2014–2039, Jun. 2011.
[3] P. Ghamisi, M. D. Mura, and J. A. Benediktsson, "A survey on spectral–spatial classification techniques based on attribute profiles," *IEEE Trans. Geosci. Remote Sens.*, vol. 53, no. 5, pp. 2335–2353, May 2015.
[4] M. Wegener, "Destriping multiple sensor imagery by improved histogram matching," *Int. J. Remote Sens.*, vol. 11, no. 5, pp. 859–875, 1990.
[5] F. L. Gadallah, F. Csillag, and E. J. M. Smith, "Destriping multisensor imagery with moment matching," *Int. J. Remote Sens.*, vol. 21, pp. 2505–2511, Aug. 2000.
[6] R. Pande-Chhetri and A. Abd-Elrahman, "De-striping hyperspectral imagery using wavelet transform and adaptive frequency domain filtering," *ISPRS J. Photogramm. Remote Sens.*, vol. 66, no. 5, pp. 620–636, 2011.
[7] H. Shen and L. Zhang, "A MAP-based algorithm for destriping and inpainting of remotely sensed images," *IEEE Trans. Geosci. Remote Sens.*, vol. 47, no. 5, pp. 1492–1502, May 2009.
[8] M. Bouali and S. Ladjal, "Toward optimal destriping of MODIS data using a unidirectional variational model," *IEEE Trans. Geosci. Remote Sens.*, vol. 49, no. 8, pp. 2924–2935, Aug. 2011.
[9] H. Zhang, W. He, L. Zhang, H. Shen, and Q. Yuan, "Hyperspectral image restoration using low-rank matrix recovery," *IEEE Trans. Geosci. Remote Sens.*, vol. 52, no. 8, pp. 4729–4743, Aug. 2014.
[10] W. He, H. Zhang, L. Zhang, and H. Shen, "Total-variation-regularized low-rank matrix factorization for hyperspectral image restoration," *IEEE Trans. Geosci. Remote Sens.*, vol. 54, no. 1, pp. 178–188, Jan. 2016.
[11] Y. Zhang and T. Zhang, "Structure-guided unidirectional variation destriping in the infrared bands of MODIS and hyperspectral images," *Infr. Phys. Technol.*, vol. 77, pp. 132–143, 2016.
[12] X. Liu, X. Lu, H. Shen, Q. Yuan, Y. Jiao, and L. Zhang, "Stripe noise separation and removal in remote sensing images by consideration of the global sparsity and local variational properties," *IEEE Trans. Geosci. Remote Sens.*, vol. 54, no. 5, pp. 3049–3060, May 2016.
[13] J. Li, Q. Yuan, H. Shen, and L. Zhang, "Hyperspectral image recovery employing a multidimensional nonlocal total variation model," *Signal Process.*, vol. 111, pp. 230–248, Jun. 2015.
[14] Y. Chang, L. Yan, H. Fang, and C. Luo, "Anisotropic spectral-spatial total variation model for multispectral remote sensing image destriping," *IEEE Trans. Image Process.*, vol. 24, no. 6, pp. 1852–1866, Jun. 2015.
[15] Y. Chang, L. Yan, T. Wu, and S. Zhong, "Remote sensing image stripe noise removal: From image decomposition perspective," *IEEE Trans. Geosci. Remote Sens.*, vol. 54, no. 12, pp. 7018–7031, Dec. 2016.
[16] W. Dong, L. Zhang, G. Shi, and X. Li, "Nonlocally centralized sparse representation for image restoration," *IEEE Trans. Image Process.*, vol. 22, no. 4, pp. 1620–1630, Apr. 2013.
[17] S. Boyd, N. Parikh, E. Chu, B. Peleato, and J. Echstein, "Distributed optimization and statistical learning via the alternating direction method of multipliers," *Found. Trends Mach. Learn.*, vol. 3, pp. 1–122, Jan. 2011.
[18] X. Zhang, M. Burger, X. Bresson, and S. Osher, "Bregmanized nonlocal regularization for deconvolution and sparse reconstruction," *SIAM J. Imag. Sci.*, vol. 3, no. 3, pp. 253–276, 2010.
[19] Z. Wang, A. C. Bovik, H. R. Sheikh, and E. P. Simoncelli, "Image quality assessment: From error visibility to structural similarity," *IEEE Trans. Image Process.*, vol. 13, no. 4, pp. 600–612, Apr. 2004.